



# Optics Letters

## Fraction-order sideband generation in an optomechanical system

JUN-HAO LIU,<sup>1</sup> GUANGQIANG HE,<sup>3</sup> QIN WU,<sup>4</sup> YA-FEI YU,<sup>2</sup> JIN-DONG WANG,<sup>2,5</sup> AND ZHI-MING ZHANG<sup>1,6</sup>

<sup>1</sup>Guangdong Provincial Key Laboratory of Nanophotonic Functional Materials and Devices (School of Information and Optoelectronic Science and Engineering), South China Normal University, Guangzhou 510006, China

<sup>2</sup>Guangdong Provincial Key Laboratory of Quantum Engineering and Quantum Materials, South China Normal University, Guangzhou 510006, China

<sup>3</sup>State Key Laboratory of Advanced Optical Communication Systems and Networks, Department of Electronic Engineering, Shanghai Jiao Tong University, Shanghai 200240, China

<sup>4</sup>School of Biomedical Engineering, Guangdong Medical University, Dongguan 523808, China

<sup>5</sup>e-mail: wangjindong@m.scnu.edu.cn

<sup>6</sup>e-mail: zhangzhiming@m.scnu.edu.cn

Received 4 June 2020; revised 11 August 2020; accepted 12 August 2020; posted 12 August 2020 (Doc. ID 399584); published 14 September 2020

**We propose a scheme for generating a new kind of sideband, i.e., the fraction-order sideband, in an optomechanical system. In the conventional scheme of high-order sideband generation [Opt. Lett. 38, 353 (2013)], the sideband interval has a minimum frequency limitation, which is equal to the mechanical frequency  $\omega_b$ , and this limits the precision of the sideband comb. With our proposed fraction-order sidebands, the sideband interval can break that limitation and reach  $\omega_b/n$  ( $n$  is an integer). The scheme we propose can be realized by driving the optomechanical system with three laser fields, including a control field ( $\omega_c$ ) and two probe fields ( $\omega_p, \omega_f$ ), in which the detuning between  $\omega_c$  and  $\omega_p$  is equal to the mechanical frequency  $\omega_b$ , while the detuning between  $\omega_c$  and  $\omega_f$  is equal to  $\omega_b/n$ . In this case, we find that not only the integer-order (high-order) sidebands, but also the fraction-order sidebands, and the sum and difference sidebands between the integer- and fraction-order sidebands, will appear in the output spectrum. Moreover, the sideband interval becomes  $\omega_b/n$ , and it can be decreased by increasing  $n$ . Our work paves the way to achieve a tunable optical frequency comb based on the optomechanical system.** © 2020 Optical Society of America

<https://doi.org/10.1364/OL.399584>

Optomechanics studies the interaction between light and mechanical oscillators via radiation pressure [1]. A typical optomechanical system consists of an optically driven Fabry–Perot cavity with one movable end-mirror, which can undergo harmonic oscillation under the influence of radiation pressure. When the driving field is incident upon the cavity, the radiation pressure will result in a displacement of the movable end-mirror, and consequently lead to a change in the cavity resonance frequency. Over the past few decades, great effort has focused on this research area for its potential application in gravitational

wave detection [2], quantum networks [3], precision measurement [4], and so on. Many important physical effects, such as normal mode splitting [5], frequency conversion [6], optomechanically induced transparency [7], cooling of the mechanical oscillator [8], entanglement, and squeezing [9,10], have been investigated in various optomechanical systems.

Recently, nonlinear effects have become the leading edge in the research of optomechanics. An interesting effect called high-order sideband generation (HSG) has drawn more and more attention for its important application in the achievement of a tunable optical frequency comb [11]. As a promising technique, tunable optical frequency combs can be applied in many engineering fields, such as precision ranging [12], tests of fundamental physics with atomic clocks [13], metrology [14], optical communication [15], and so on. In 2013, Xiong *et al.* first demonstrate the HSG in an ultrastrong driven optomechanical system beyond the perturbative approximation [16]. Whereafter, people explored many other physical effects and systems combined with optomechanical systems, such as the Coulomb effect [17], atomic ensemble [18], Casimir effect [19], and parity–time symmetry structure [20], to enhance the HSG.

In the above conventional schemes of HSG, the sideband interval is equal to the mechanical frequency  $\omega_b$ . For a practical optomechanical microcavity, its mechanical eigenfrequency is usually fixed. That is to say, the sideband interval is untunable and has a minimum frequency limitation  $\omega_b$ , and this limits the precision of the sideband comb. Here we propose a new kind of sideband, i.e., the fraction-order sideband, which can be used to break that limitation, and the sideband interval becomes  $\omega_b/n$  ( $n$  is an integer). Our proposed scheme is based on an optomechanical system driven by a control field ( $\omega_c$ ) and two probe fields ( $\omega_p, \omega_f$ ), where the detuning between  $\omega_c$  and  $\omega_p$  ( $\omega_f$ ) is equal to the mechanical frequency  $\omega_b$  ( $\omega_b/n$ ). In this case, the output spectrum consists of a series of integer-order (high-order) sidebands, fraction-order sidebands, as well as the

sum and difference sidebands between the integer- and fraction-order sidebands, and the sideband interval can be decreased by increasing  $n$ .

Our proposed scheme is shown in Fig. 1(a). We consider a standard model of an optomechanical system where an optical cavity mode  $\hat{a}$  parametrically couples with a mechanical mode  $\hat{b}$  via radiation pressure. The cavity mode is pumped by a control field  $\omega_c$  and two probe fields  $\omega_p$  and  $\omega_f$ . The Hamiltonian of the system can be expressed as ( $\hbar = 1$ )

$$H = \omega_a \hat{a}^\dagger \hat{a} + \omega_b \hat{b}^\dagger \hat{b} + g \hat{a}^\dagger \hat{a} (\hat{b}^\dagger + \hat{b}) + i[\hat{a}^\dagger (\varepsilon_c e^{-i\omega_c t} + \varepsilon_p e^{-i\omega_p t} + \varepsilon_f e^{-i\omega_f t}) - \text{H.c.}], \quad (1)$$

where  $\hat{a}$  ( $\hat{a}^\dagger$ ) and  $\hat{b}$  ( $\hat{b}^\dagger$ ) are the bosonic annihilation (creation) operators for the cavity mode and the mechanical mode with frequencies  $\omega_a$  and  $\omega_b$ , respectively.  $g = x_{zpf} \omega_a / L$  is the single-photon optomechanical coupling strength, where  $x_{zpf} = \sqrt{\hbar / 2m\omega_b}$  is the zero-point fluctuation,  $m$  is the mass of the mechanical oscillator, and  $L$  is the length of the cavity. The amplitude of the driving field is  $\varepsilon_y = \sqrt{2\kappa P_y / \hbar \omega_y}$  ( $y = c, p, f$ ), in which  $\kappa$  denotes the cavity damping rate, and  $P_y$  refers to the corresponding input power.

Based on the Hamiltonian (1), the evolution of the system can be described by the Heisenberg–Langevin equations (in a frame rotating at the frequency  $\omega_c$ )

$$\frac{d\hat{a}}{dt} = -(i\Delta_a + \kappa)\hat{a} - ig\hat{a}(\hat{b}^\dagger + \hat{b}) + \varepsilon_c + \varepsilon_p e^{-i\delta_p t} + \varepsilon_f e^{-i\delta_f t} + \sqrt{2\kappa}\hat{a}_{in}, \quad (2)$$

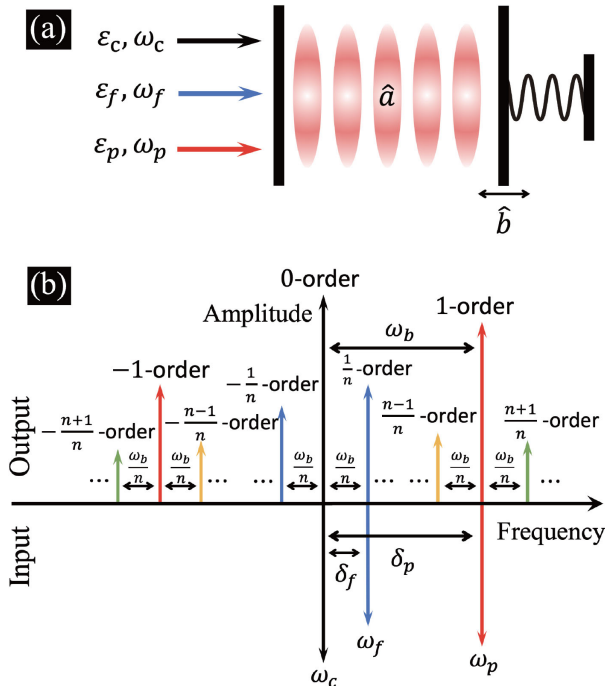


**Fig. 1.** (a) Standard optomechanical system driven by a control field ( $\omega_c$ ) and two probe fields ( $\omega_p, \omega_f$ ). (b) Schematic diagram of the nonlinear sideband generation. We exhibit the integer-order sidebands (zeroth-order,  $\pm 1$ -order), the fraction-order sidebands ( $\pm 1/n$ -order), the sum and difference sidebands ( $\pm \frac{n\pm 1}{n}$ -order).

$$\frac{d\hat{b}}{dt} = -(i\omega_b + \gamma)\hat{b} - ig\hat{a}^\dagger \hat{a} + \sqrt{2\gamma}\hat{b}_{in}, \quad (3)$$

where  $\Delta_a = \omega_a - \omega_c$  is the frequency detuning between the control field  $\omega_c$  and the cavity field  $\omega_a$ .  $\delta_p = \omega_p - \omega_c$  ( $\delta_f = \omega_f - \omega_c$ ) is the frequency detuning between the control field  $\omega_c$  and the probe field  $\omega_p$  ( $\omega_f$ ).  $\gamma$  is the mechanical damping rate.  $\hat{a}_{in}$  and  $\hat{b}_{in}$  are, respectively, the fluctuation operations corresponding to the cavity mode and the mechanical mode with zero mean value, i.e.,  $\langle \hat{a}_{in} \rangle = \langle \hat{b}_{in} \rangle = 0$ . In this Letter, we focus on the mean response of the system to the probe fields; thus, in the following, we turn to calculate the evolution of the expectation values of the system operators  $\hat{a}$  and  $\hat{b}$ , and we denote  $\langle \hat{a} \rangle \equiv \alpha$ ,  $\langle \hat{b} \rangle \equiv \beta$ . By using the mean-field approximation, i.e.,  $\langle \hat{a}\hat{b} \rangle = \langle \hat{a} \rangle \langle \hat{b} \rangle$ , the dynamical equations of the system can be derived from Eqs. (2) and (3) as

$$\frac{d\alpha}{dt} = -(i\Delta_a + \kappa)\alpha - ig\alpha(\beta + \beta^*) + \varepsilon_c + \varepsilon_p e^{-i\delta_p t} + \varepsilon_f e^{-i\delta_f t}, \quad (4)$$

$$\frac{d\beta}{dt} = -(i\omega_b + \gamma)\beta - ig|\alpha|^2. \quad (5)$$

We recall that the solutions to the above nonlinear equations have been addressed in previous works for the following three parametric conditions: (i)  $\varepsilon_f = 0$ ,  $\varepsilon_p \neq 0$ ,  $\varepsilon_p / \varepsilon_c \ll 1$ ; under this circumstance, the equations can be solved by using the so-called linearization method, and the Stokes and anti-Stokes processes are discussed [21]. (ii)  $\varepsilon_f \neq 0$ ,  $\varepsilon_p \neq 0$ ,  $\varepsilon_p / \varepsilon_c \ll 1$ ,  $\varepsilon_f / \varepsilon_c \ll 1$ ; in this case, the linearization is practicable, and the sum and difference sideband effects are investigated [22,23]. (iii)  $\varepsilon_f = 0$ ,  $\varepsilon_p \neq 0$ ,  $\varepsilon_p \sim \varepsilon_c$ ; in this regime, the linearization is inapplicable, and the high-order sideband effect is studied by using numerical calculation [16].

In this Letter, we study the fourth circumstance, i.e.,  $\varepsilon_p \neq 0$ ,  $\varepsilon_f \neq 0$ ,  $\varepsilon_f \sim \varepsilon_p \sim \varepsilon_c$ . Different from the previous cases, here the expectation value  $x(x = \alpha, \beta)$  is written as the following ansatz:  $x = x_0 + x_p + x_f + x_s + x_d$ , where  $x_0$  denotes the steady-state solution when  $\varepsilon_p = \varepsilon_f = 0$ . The optomechanical nonlinearity [corresponding to the terms  $-ig|\alpha|^2$  and  $-ig\alpha(\beta^* + \beta)$ ] will result in the generation of new photons with different frequencies. When the laser fields are incident upon the cavity, the driving energy will be transferred to a series of sidebands with new frequencies, which can be expressed as

$$x_p = \sum_{j=1}^N x_{p+}^{(j)} e^{-ij\delta_p t} + x_{p-}^{(j)} e^{ij\delta_p t}, \quad (6)$$

$$x_f = \sum_{k=1}^M x_{f+}^{(k)} e^{-ik\delta_f t} + x_{f-}^{(k)} e^{ik\delta_f t}. \quad (7)$$

Similar to the sum and difference frequency generations in the nonlinear medium [24], a series of sum and difference sidebands can be generated in our optomechanical system, which are written as

$$x_s = \sum_{j=1}^N \sum_{k=1}^M x_{s+}^{(j,k)} e^{-i(j\delta_p + k\delta_f)t} + x_{s-}^{(j,k)} e^{i(j\delta_p + k\delta_f)t}, \quad (8)$$

$$x_d = \sum_{j=1}^N \sum_{k=1}^M x_{d+}^{(j,k)} e^{-i(j\delta_p - k\delta_f)t} + x_{d-}^{(j,k)} e^{i(j\delta_p - k\delta_f)t}. \quad (9)$$

By solving Eqs. (4) and (5) with the help of the ansatz, and using the input–output relation [25]  $S_{\text{out}} = S_{\text{in}} - \sqrt{2\kappa}\alpha$  ( $S_{\text{in}} = \varepsilon_c + \varepsilon_p e^{-i\delta_p t} + \varepsilon_f e^{-i\delta_f t}$ ), we can finally obtain the output spectrum of the system:  $S_{\text{out}} = S_0 + S_p + S_f + S_s + S_d$ , in which we have assumed that the detunings between the probe fields and the control field satisfy: (i)  $\delta_p = \omega_b$ ; (ii)  $\delta_f = \omega_b/n$  ( $n$  is an integer). It should be noted that the spectra obtained have shifted the frequency  $\omega_c$ , because Eqs. (4) and (5) describe the evolution of the optical field in a frame rotating at the control frequency. The output spectrum includes the following five parts, as shown in Fig. 1(b): the first part  $S_0 = \varepsilon_c - \sqrt{2\kappa}\alpha_0$  is the zeroth-order sideband, which corresponds to the control field  $\omega_c$ . The second and third parts denote the integer- and fraction-order sidebands, respectively, which can be expressed as

$$S_p = \sum_{j=1}^N A_{p+}^{(j)} e^{-ij\omega_b t} + A_{p-}^{(j)} e^{ij\omega_b t}, \quad (10)$$

$$S_f = \sum_{k=1}^M A_{f+}^{(k)} e^{-i\frac{k}{n}\omega_b t} + A_{f-}^{(k)} e^{i\frac{k}{n}\omega_b t}, \quad (11)$$

and we will see a series of sidebands appear at  $\omega = \pm j\omega_b$  and  $\omega = \pm \frac{k}{n}\omega_b$ , in which  $A_{p+}^{(1)}$  and  $A_{f+}^{(1)}$  are called the first- and  $\frac{1}{n}$ -order sidebands, which correspond to the probe field  $\omega_p$  and  $\omega_f$ , respectively. The fourth and fifth parts describe the sum and difference sidebands, respectively, which are given by

$$S_s = \sum_{j=1}^N \sum_{k=1}^M A_{s+}^{(j,k)} e^{-i\frac{jn+k}{n}\omega_b t} + A_{s-}^{(j,k)} e^{i\frac{jn+k}{n}\omega_b t}, \quad (12)$$

$$S_d = \sum_{j=1}^N \sum_{k=1}^M A_{d+}^{(j,k)} e^{-i\frac{jn-k}{n}\omega_b t} + A_{d-}^{(j,k)} e^{i\frac{jn-k}{n}\omega_b t}. \quad (13)$$

That means a series of new fraction-order sidebands will appear at  $\omega = \pm \frac{jn \pm k}{n}\omega_b$ , and we call  $A_{s\pm}^{(j,k)}$  and  $A_{d\pm}^{(j,k)}$  as the  $\pm \frac{jn+k}{n}$ - and  $\pm \frac{jn-k}{n}$ -order sidebands, respectively.

It can be seen that it is very difficult and tedious to give the analytical solutions to the sidebands for every order. To verify our theory and exhibit all the generated sidebands, a more convenient practice is to use numerical calculation, and we adopt the Runge–Kutta method to solve Eqs. (4) and (5), then the output spectrum can be obtained by using the fast Fourier transform. The used parameters are chosen based on a recent experiment [26] and can be achieved under current technology:  $\omega_b/2\pi = 51.8$  MHz and  $\gamma/2\pi = 41$  kHz (quality factor  $Q_m = 1.26 \times 10^3$ ),  $m = 20$  ng,  $\Delta_a = \omega_b$ ,  $\kappa/2\pi = 15$  MHz,  $g/2\pi = 1$  kHz, the wavelength of the control field  $\lambda_c = 795$  nm, and  $\varepsilon_c = 3 \times 10^3$  GHz.

To exhibit the sideband generation output from the system, we first assume that  $\varepsilon_f = 0$  and show the integer-order (high-order) sideband spectra in Fig. 2. We can see that when  $\varepsilon_p$  is weak ( $\varepsilon_p/\varepsilon_c = 3 \times 10^{-2}$ ), there are only zeroth-order and  $\pm 1$ -order sidebands in the output spectrum. If we increase  $\varepsilon_p$

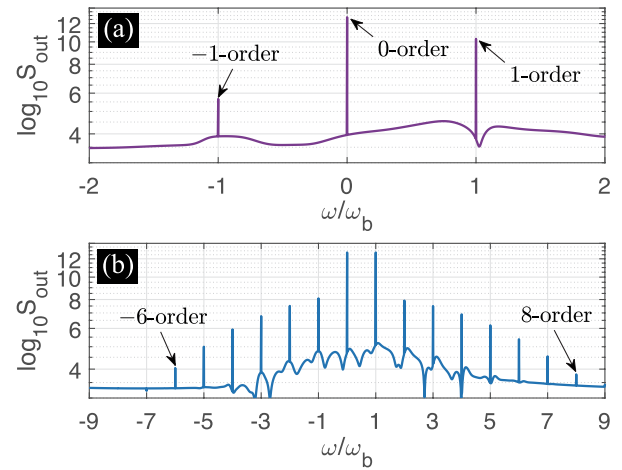


**Fig. 2.** Integer-order sideband spectra for different  $\varepsilon_p$ : (a)  $\varepsilon_p = 9$  GHz, (b)  $\varepsilon_p = 3 \times 10^3$  GHz, and the other parameters are stated in the text.

and when  $\varepsilon_p$  is strong ( $\varepsilon_p/\varepsilon_c = 1$ ), the amplitudes of  $\pm 1$ -order sidebands are strengthened, and the higher integer-order sidebands appear, the positive and negative sidebands end up at the orders of  $+8$  and  $-6$ , respectively. Furthermore, for a higher order of the sideband, the amplitude is smaller. In general, both the cutoff-order number and the amplitude will gradually increase with the increasing of  $\varepsilon_p$ . However, the sideband interval does not change and is always  $\omega_b$ .

Below we show the integer-order and fraction-order sideband spectra for different  $n$ , as shown in Fig. 3. We consider that another probe field  $\omega_f$  is inputted into the cavity with a very small amplitude ( $\varepsilon_f/\varepsilon_c = 3 \times 10^{-3}$ ), and the other conditions

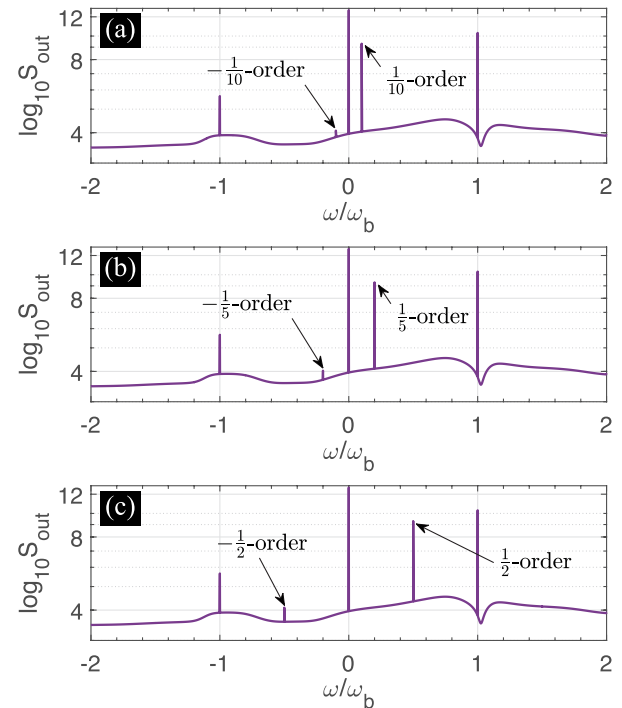


**Fig. 3.** Integer-order and fraction-order sideband spectra for different  $n$ : (a)  $n = 10$ , (b)  $n = 5$ , and (c)  $n = 2$ .  $\varepsilon_f = 9 \times 10^{-1}$  GHz, and the other parameters are the same as those in Fig. 2(a).

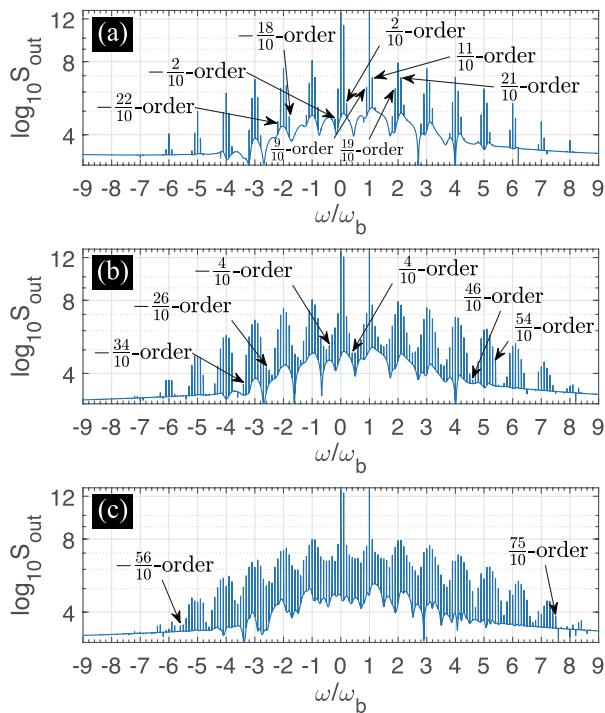


**Fig. 4.** Higher integer-order, fraction-order, sum and difference sideband spectra for different  $\varepsilon_f$ : (a)  $\varepsilon_f = 9 \times 10^1$  GHz, (b)  $\varepsilon_f = 6 \times 10^2$  GHz, and (c)  $\varepsilon_f = 1.2 \times 10^3$  GHz.  $n = 10$ , and the other parameters are the same as those in Fig. 2(b).

are the same as in Fig. 2(a). It can be seen that the integer-order sidebands have hardly changed, while two new fraction-order sidebands appear, and their positions depend on  $n$ . Especially when  $n = 2$ , the newly generated  $\pm \frac{1}{2}$ -order sidebands and the pre-existing zeroth-order and  $\pm 1$ -order sidebands constitute a series of new equidistant sidebands, and the sideband interval becomes half of the mechanical frequency.

Figure 4 displays the higher integer-order, fraction-order, sum and difference sideband spectra for different  $\varepsilon_f$ , and the other conditions are the same as in Fig. 2(b). When  $\varepsilon_f/\varepsilon_c = 3 \times 10^{-2}$ , the amplitudes of  $\pm \frac{1}{10}$ -order sidebands are obviously enhanced compared with those in Fig. 3(a), and the sum and difference sidebands between  $\pm \frac{1}{10}$ -order and the integer-order sidebands, such as  $\pm \frac{11}{10}$ -order,  $\pm \frac{9}{10}$ -order,  $\pm \frac{19}{10}$ -order,  $\pm \frac{21}{10}$ -order sidebands, etc., appear in the output spectrum. Furthermore, the higher fraction-order sidebands, such as  $\pm \frac{2}{10}$ -order sidebands, come out, and the sum and difference sidebands between  $\pm \frac{2}{10}$ -order and the integer-order sidebands can also be seen, e.g.,  $\pm \frac{18}{10}$ -order,  $-\frac{22}{10}$ -order sidebands, etc. When  $\varepsilon_f/\varepsilon_c = 2 \times 10^{-1}$ , there are more higher fraction-order sidebands, such as  $\pm \frac{4}{10}$ -order sidebands, and more sum and difference sidebands, such as  $-\frac{46}{10}$ -order sidebands. If we continue to increase  $\varepsilon_f$  and when  $\varepsilon_f/\varepsilon_c = 4 \times 10^{-1}$ , it can be seen that more sum and difference sidebands appear, e.g.,  $-\frac{56}{10}$ -order and  $\frac{75}{10}$ -order sidebands. In this case, the sideband range is approximately equal to that in Fig. 2(b), while the sideband interval is decreased by one order of magnitude.

In summary, this Letter proposed a new kind of sideband, i.e. the fraction-order sideband, which can be generated in an optomechanical system driven by a control field ( $\omega_c$ ) and two probe fields ( $\omega_p, \omega_f$ ), where the detuning between  $\omega_c$  and  $\omega_p$  ( $\omega_f$ ) is equal to the mechanical frequency  $\omega_b$  ( $\omega_b/n$ ). The most significant advantage of fraction-order sidebands is that they can enable us to decrease the sideband interval by increasing  $n$ . We conclude that the challenge to achieve a tunable optical frequency comb based on the optomechanical system will be greatly aided by our work.

**Funding.** National Natural Science Foundation of China (11574092, 61378012, 61475099, 61775062, 61941501, 91121023); Program of State Key Laboratory of Quantum Optics and Quantum Optics Devices (KF201701); Doctoral Program of Guangdong Natural Science Foundation (2018A030310109).

**Disclosures.** The authors declare no conflicts of interest.

## REFERENCES

1. M. Aspelmeyer, T. J. Kippenberg, and F. Marquardt, *Rev. Mod. Phys.* **86**, 1391 (2014).
2. H. Miao, Y. Ma, C. Zhao, and Y. Chen, *Phys. Rev. Lett.* **115**, 211104 (2015).
3. K. Stannigel, P. Rabl, A. S. Sørensen, P. Zoller, and M. D. Lukin, *Phys. Rev. Lett.* **105**, 220501 (2010).
4. G. A. Brawley, M. R. Vanner, P. E. Larsen, S. Schmid, A. Boisen, and W. P. Bowen, *Nat. Commun.* **7**, 10988 (2016).
5. M. Rossi, N. Kralj, S. Zippilli, R. Natali, A. Borrielli, G. Pandraud, E. Serra, G. D. Giuseppe, and D. Vitali, *Phys. Rev. Lett.* **120**, 073601 (2018).
6. J. T. Hill, A. H. Safavi-Naeini, J. Chan, and O. Painter, *Nat. Commun.* **3**, 1196 (2012).
7. A. Kronwald and F. Marquardt, *Phys. Rev. Lett.* **111**, 133601 (2013).
8. Y. L. Liu and Y. X. Liu, *Phys. Rev. A* **96**, 023812 (2017).
9. J. H. Liu, Y. B. Zhang, Y. F. Yu, and Z. M. Zhang, *Opt. Express* **25**, 7592 (2017).
10. B. Xiong, X. Li, S. L. Chao, and L. Zhou, *Opt. Lett.* **43**, 6053 (2018).
11. H. Xiong, L. G. Si, X. Y. Lü, X. Yang, and Y. Wu, *Ann. Phys.* **349**, 43 (2014).
12. K. Minoshima and H. Matsumoto, *Appl. Opt.* **39**, 5512 (2000).
13. T. Rosenband, D. B. Hume, P. O. Schmidt, C. W. Chou, A. Brusch, L. Lorini, W. H. Oskay, R. E. Drullinger, T. M. Fortier, J. E. Stalnaker, S. A. Diddams, W. C. Swann, N. R. Newbury, W. M. Itano, D. J. Wineland, and J. C. Bergquist, *Science* **319**, 1808 (2008).
14. J. L. Hall, *Rev. Mod. Phys.* **78**, 1279 (2006).
15. N. G. Pavlov, G. Lihachev, S. Koptyaev, E. Lucas, M. Karpov, N. M. Kondratiev, I. A. Bilenko, T. J. Kippenberg, and M. L. Gorodetsky, *Opt. Lett.* **42**, 514 (2017).
16. H. Xiong, L. G. Si, X. Y. Lü, X. X. Yang, and Y. Wu, *Opt. Lett.* **38**, 353 (2013).
17. C. Kong, H. Xiong, and Y. Wu, *Phys. Rev. A* **95**, 033820 (2017).
18. Z. X. Liu, H. Xiong, and Y. Wu, *Phys. Rev. A* **97**, 013801 (2018).
19. J. Yao, Y. F. Yu, and Z. M. Zhang, *Chin. Opt. Lett.* **16**, 111201 (2018).
20. L. Y. He, *Phys. Rev. A* **99**, 033843 (2019).
21. S. Huang and G. S. Agarwal, *Phys. Rev. A* **81**, 033830 (2010).
22. H. Xiong, L. G. Si, X. Y. Lü, and Y. Wu, *Opt. Express* **24**, 5773 (2016).
23. H. Xiong, Y. W. Fan, X. X. Yang, and Y. Wu, *Appl. Phys. Lett.* **109**, 061108 (2016).
24. J. Wang, J. Sun, C. Luo, and Q. Sun, *Opt. Express* **13**, 7405 (2005).
25. C. W. Gardiner and M. J. Collett, *Phys. Rev. A* **31**, 3761 (1985).
26. S. Weis, R. Rivière, S. Deléglise, E. Gavartin, O. Arcizet, A. Schliesser, and T. J. Kippenberg, *Science* **330**, 1520 (2010).